Chapter 6

Modeling and experimental validation of the optimal positioning of reference electrode for a Silicon Nitride gate pH ISFET

6.1 Introduction

Precise *in-vivo* measurements are the primary requisite for implantable sensors. Challenges such as biocompatibility, cost-effectiveness, compactness, minimally invasiveness etc. proves to be a hurdle in the path of development of such sensors. ISFET based sensors can be used for both *in-vivo* and *in-vitro* measurements. The reference electrode which completes the gate to source circuit is an inseparable part of it. The positioning of the reference electrode is very crucial, as the proper knowledge of its position can help in reducing device dimensions and hence make the device compact. This can be extended to all related ISFET based sensors. A theoretical model was proposed in 2009, which defined that the optimal positioning of the reference electrode should be three or more than three times of the Debye length for each respective pH values of the measurand [1]. The model was proposed for silicon dioxide. In this chapter, it is extended for silicon nitride sensing surface and the validation of the theoretical data is done with the experimentally obtained values. This validation of the theoretical model can prove to be a milestone in designing biomedical sensors and also can be put to use for the reference electrode positioning for the ENFET designed in the previous chapter.

6.2 Theory

The ISFET device as already stated so far clearly indicates that it is devoid of the gate over layer hence it necessarily requires a reference electrode to complete the gate to source circuit [2]. The reference electrode should be an ideal non-polarizable electrode. The voltage applied to the reference electrode predominantly controls the conductance of the device. The applied voltage to the reference electrode dictates the state of the device i.e. if it is in active or saturation mode. Any change in the surface interfacial potential can be detected by the observed change in drain current. The position of the reference electrode can affect this interfacial potential. As indicated in the theoretical model, when the electrode is moved to the bulk of the solution the potential gradually decreases and attains a stable value [3]. When the electrode is placed at the close vicinity of the sensing layer, the effective insulator electrolyte potential is incomplete.

Therefore, to obtain the complete model of ISFET response, the interfacial insulator electrolyte potential is to be expressed as a function of the position of the reference electrode with respect to the sensing layer.

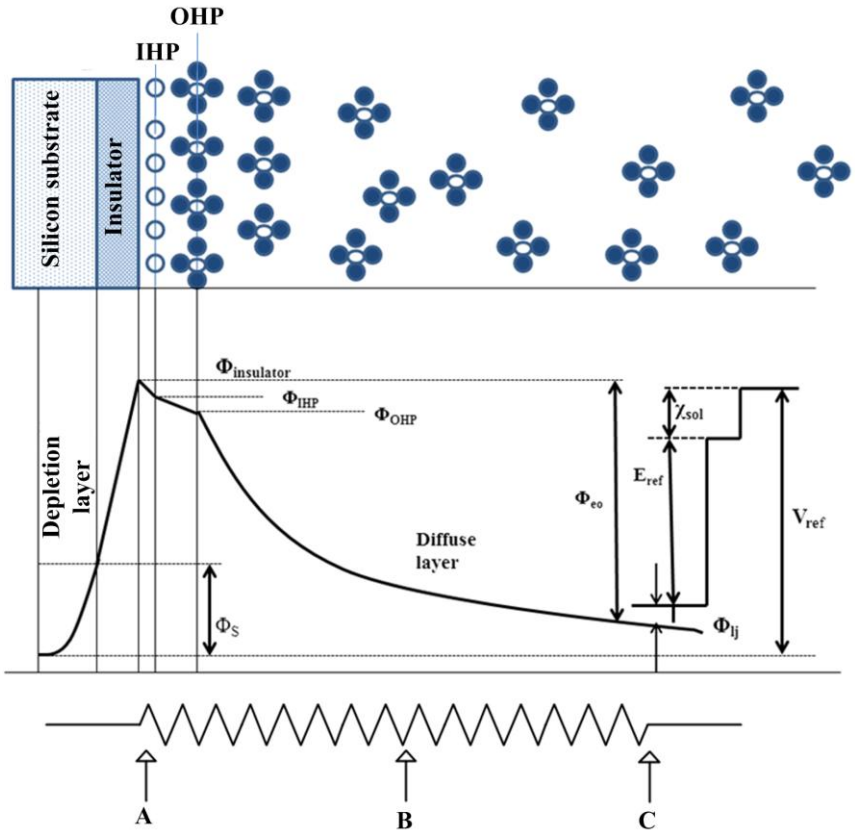

Figure 6.1.Figure depicting the potential profile of the EIS structure for a planar surface when the reference electrode is placed in the bulk of the solution [1]

When the reference electrode is placed in the bulk of the solution the potential profile of the electrolyte insulator semiconductor (EIS) structure for a planar surface varies as illustrated in figure 6.1. The electrolyte considered is having pH value greater than pH_{PZC}. The potential decreases exponentially and becomes steady in the bulk of the solution. The surface potential at the semiconductor is denoted as ϕ_s. The potential variation across the diffused layer can be explained using an analogy of a variable resistor as illustrated in figure 6.1. Considering reference electrode to be the slider 'B' advancing towards 'C' and departing away from point 'A', the effect of this movement can be explained by an increase in resistance between point A and B, consequently leading to a decrease in the resistance between point B and C. Here point 'A' is analogous to

the sensing layer and the point 'C' describes three times of the Debye length as proposed in the theoretical model [1]. In figure 6.1 the ϕ_{eo} when considered as the potential across the considered resistance, placing of the reference electrode at point 'C' can provide with the full range of ϕ_{eo}.

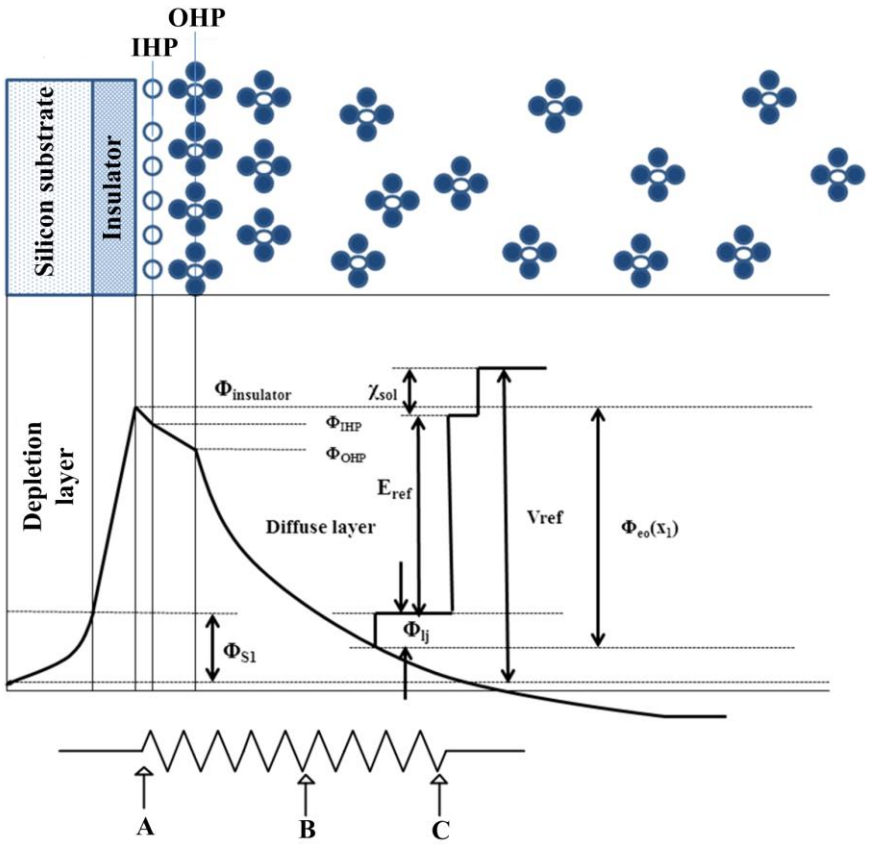

Figure 6.2. Figure depicting the potential profile of the EIS structure for a planar surface when the reference electrode is placed in the diffused layer [1]

Further, from figure 6.2 it can be observed that the full range of ϕ_{eo} is not achievable when the reference electrode is placed within the diffuse layer i.e. before point 'C'. Here ϕ_{s1} denotes the semiconductor surface potential. Both figures 6.1 and 6.2 clearly suggests that $\phi_{s1} < \phi_S$. Lesser charge at the inversion layer is therefore developed as the result of decreased semiconductor potential leading to subsequent drop in the magnitude of the drain current. Hence as depicted in figure 6.2 the potential profile obtained is incomplete. In the earlier proposed theoretical model silicon dioxide was being considered as sensing layer. Here in this chapter, the model is extended further to silicon nitride and the

mathematical modeling has been carried out. Here in the following the mathematical modeling for silicon nitride is stated, followed by the methodology involved for the validation of this theoretical model.

6.3 Mathematical modeling

In Si_3N_4 gate pH ISFET, the insulating layer consists of two types of different groups of active sites i.e. silanol and amine groups as depicted in figure 6.3. As stated earlier in chapter 2, the exchange of hydrogen ion takes place between the active sites and the constituent ions present in the electrolyte [2]. This result into redistribution of charges in the electrical double layer (EDL) formed in the vicinity of the insulator layer when immersed in the electrolyte. The redistribution of charges in this EDL affects the flat-band voltage which in turn modifies the threshold voltage of ISFET device. The threshold voltage stated in equation 3.22 (excluding the trapped charges, interface charges and the fixed immobile charges) indicates that all the terms present are constant except the interfacial insulator electrolyte potential (ϕ_{eo}). Therefore, it can be said that the interfacial insulator electrolyte potential influences the ISFET response. Here for silicon nitride surface, a mathematical relation between the interfacial insulator electrolyte potential (ϕ_{eo}) and the distance (x) of the reference electrode from the OHP has been established.

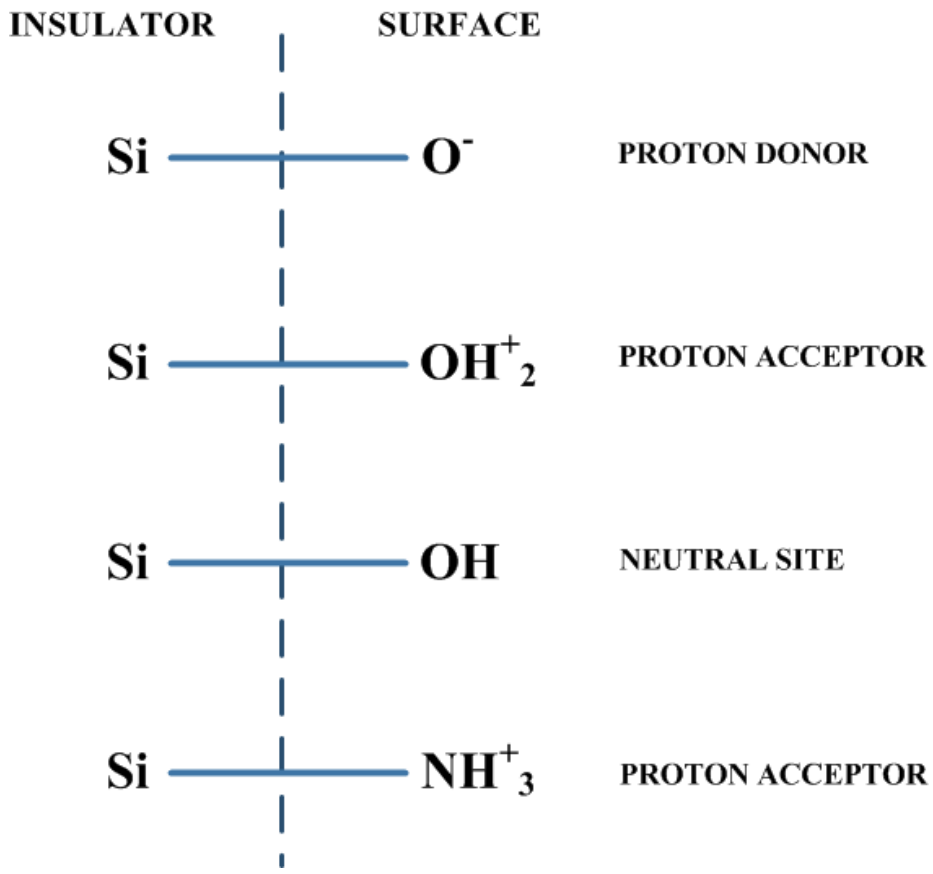

Figure 6.3.Site binding model of the silicon nitride surface

6.3.1 Model description

The insulating surface of silicon nitride when in contact of water, yields the silanol SiOH and amine $SiNH_2$ sites according to the schematic reactions [3, 4, 5, 6].

$$Si_3N(s) + H_2O(l) \leftrightarrow Si_2NH(s) + SiOH(s) \quad (6.1)$$

$$Si_2NH(s) + H_2O(l) \leftrightarrow SiNH_2(s) + SiOH(s) \quad (6.2)$$

Here *s* and *l* indicate solid and liquid phase respectively. Here in the model only those surface sites which are involved in the absorption or desorption of hydrogen ion are considered.

In an acidic environment (pH≤7), silanol and amine sites adsorb and desorb protons according to the following reactions [5, 6, 7]

$$SiNH_2(s) + H^+(l) \leftrightarrow SiNH_3^+(s) \tag{6.3}$$

$$SiOH(s) + H^+(l) \leftrightarrow SiOH_2^+(s) \tag{6.4}$$

$$SiOH(s) \leftrightarrow SiO^-(s) + H^+(l) \tag{6.5}$$

At thermodynamic equilibrium,

$$K_N[SiNH_2][H^+] = [SiNH_3^+] \tag{6.6}$$

$$K_S^+[SiOH][H^+] = [SiOH_2^+] \tag{6.7}$$

Here $[H^+]$ denotes concentration of protons. K_N, K^+_S and K^-_S are the relative equilibrium constant values, which are found to be [8, 9, 10, 11]

$K_N \approx 7.7 \times 10^9$, $K^+_S \approx 6.3 \times 10$, $K^-_S \approx 63.1 \times 10^{-9}$, $N_S \approx 5 \times 10^{14}\text{cm}^{-2}$

6.3.2. Model formulation

The response of the reference electrode is related to the interfacial electrode potential which is already mentioned above. Further, the surface potential is related to the pH value of the electrolyte. So, when the pH < pH_{PZC} the surface is positively charged. Conversely, when pH > pH_{PZC} the surface gets negatively charged. The potential of the diffuse layer can be stated by the Poisson Boltzmann equation for a planar surface along with the following boundary conditions given as-

$$\frac{d^2\phi}{dx^2} = -\frac{\sum_{i=1}^{N} C_i^{bulk} z_i q e^{-\frac{Z_i q\phi}{K_B T}}}{\varepsilon_o \varepsilon_r} \tag{6.8}$$

The boundary conditions are [12]

$$\left.\frac{d\phi}{dx}\right|_{x=0} = -\frac{\rho}{\varepsilon_o \varepsilon_r} > 0 \qquad \text{when pH} < pH_{PZC}$$

$$\left.\frac{d\phi}{dx}\right|_{x=0} = -\frac{\rho}{\varepsilon_o \varepsilon_r} < 0 \qquad \text{when pH} > pH_{PZC}$$

With the following transformation for equation (6.8)

$$\frac{d^2\phi}{dx^2} = \frac{1}{2}\frac{d}{d\phi}\left(\frac{d\phi}{dx}\right)^2 \tag{6.9}$$

Therefore, equation (6.8) can be written as-

$$\frac{1}{2}\frac{d}{d\phi}\left(\frac{d\phi}{dx}\right)^2 = -\frac{\sum_{i=1}^{N} C_i^{bulk} z_i q e^{-\frac{Z_i q\phi}{K_B T}}}{\varepsilon_o \varepsilon_r} \tag{6.10}$$

Integrating equation (6.10) –

$$\int \frac{1}{2}\frac{d}{d\phi}\left(\frac{d\phi}{dx}\right)^2 = -\int \frac{\sum_{i=1}^{N} C_i^{bulk} z_i q e^{-\frac{Z_i q\phi}{K_B T}}}{\varepsilon_o \varepsilon_r}$$

$$\frac{1}{2}\left(\frac{d\phi}{dx}\right)^2 = \frac{K_B T}{\varepsilon_o \varepsilon_r}\sum_{i=1}^{N} C_i^{bulk} e^{-\frac{Z_i q\phi}{K_B T}} + C_1$$

$$\left(\frac{d\phi}{dx}\right)^2 = \frac{2K_B T}{\varepsilon_o \varepsilon_r}\sum_{i=1}^{N} C_i^{bulk} e^{-\frac{Z_i q\phi}{K_B T}} + C_1 \tag{6.11}$$

Using the boundary conditions

$x = 0$, $\phi = \phi_{eo}$, $x = \infty$, $\phi = 0$, $d\phi/dx = 0$

Applying the above conditions, constant is obtained.

$$C_1 = -\frac{2K_B T}{\varepsilon_o \varepsilon_r}\sum_{i=1}^{N} C_i^{bulk} \tag{6.12}$$

From equation (6.11) and (6.12) we can have the following form of equation

$$\left(\frac{d\phi}{dx}\right)^2 = \frac{2K_BT}{\varepsilon_o\varepsilon_r}\sum_{i=1}^{N} C_i^{bulk}\left(e^{-\frac{z_i q\phi}{K_BT}} - 1\right) \tag{6.13}$$

Since, 1:1 electrolyte has been considered

$$|z_+| = |z_-| = z = 1$$

Where z is valency

$$C_+^{bulk} = C_-^{bulk} = C^{bulk}$$

Hence N=3 (two for cationic and one for anionic)

$$\left(\frac{d\phi}{dx}\right)^2 = \frac{2K_BT}{\varepsilon_o\varepsilon_r}C^{bulk}\left(e^{\frac{zq\phi}{K_BT}} - 1 + e^{-\frac{zq\phi}{K_BT}} - 1 + e^{-\frac{zq\phi}{K_BT}} - 1\right)$$

$$\left(\frac{d\phi}{dx}\right)^2 = \frac{2K_BT}{\varepsilon_o\varepsilon_r}C^{bulk}\left(2e^{-\frac{zq\phi}{K_BT}} + e^{\frac{zq\phi}{K_BT}} - 3\right)$$

$$\left(\frac{d\phi}{dx}\right)^2 = \frac{2K_BT}{\varepsilon_o\varepsilon_r}C^{bulk}\left(-\sinh\left(\frac{zq\phi}{K_BT}\right) + 3\cosh\left(\frac{zq\phi}{K_BT}\right) - 3\right)$$

For simplicity –

$$\cosh\left(\frac{zq\phi}{K_BT}\right) \approx 1 + \frac{1}{2}\left(\frac{zq\phi}{K_BT}\right)^2$$

$$\sinh\left(\frac{zq\phi}{K_BT}\right) \approx \frac{zq\phi}{K_BT}$$

$$\left(\frac{d\phi}{dx}\right)^2 = \frac{2K_BT}{\varepsilon_o\varepsilon_r}C^{bulk}\left\{\frac{3}{2}\left(\frac{zq\phi}{K_BT}\right)^2 - \frac{zq\phi}{K_BT}\right\} \tag{6.14}$$

$$\frac{d\phi}{dx} = \pm\left[\left(\frac{2K_BTC^{bulk}z^2q^2}{\varepsilon_o\varepsilon_rK_BT}\right)\left(\frac{3}{2}\phi^2 - \frac{K_BT}{zq}\phi\right)\right]^{\frac{1}{2}} \tag{6.15}$$

Since, electric field is negative gradient of potential here we consider only the negative term. Therefore equation (6.15) becomes

$$\frac{d\phi}{dx} = -\left[\left(\frac{2C^{bulk}z^2q^2}{\varepsilon_o\varepsilon_rK_BT}\right)\left(\frac{3}{2}\phi^2 - \frac{K_BT}{zq}\phi\right)\right]^{\frac{1}{2}}$$

$$\frac{d\phi}{dx} = -\frac{1}{L_D}\left[\left(\frac{3}{2}\phi^2 - \frac{K_BT}{zq}\phi\right)\right]^{\frac{1}{2}}$$

$$\frac{d\phi}{dx} = -\frac{1}{L_D}\left(\frac{3}{2}\right)^{\frac{1}{2}}\left(\phi - \frac{K_BT}{3zq}\right) \tag{6.16}$$

Again, it can be assumed that

$$\phi - \frac{K_BT}{3zq} \approx \phi \tag{6.17}$$

Therefore equation (6.16) becomes

$$\frac{d\phi}{dx} = -\frac{1}{L_D}\left(\frac{3}{2}\right)^{\frac{1}{2}}\phi$$

$$\int\frac{d\phi}{\phi} = -\left(\frac{3}{2}\right)^{\frac{1}{2}}\frac{1}{L_D}\int dx$$

$$\ln(\phi) = -\left(\frac{3}{2}\right)^{\frac{1}{2}}\frac{1}{L_D}x + C_2$$

$$\phi = \exp\left[-\left(\frac{3}{2}\right)^{\frac{1}{2}} \frac{x}{L_D}\right].C_2 \tag{6.18}$$

Now following the boundary condition x=0, $\phi = \phi_{e0}$, and $x = \infty$, $\phi = 0$

$$\phi_{eo} = C_2$$

Therefore, we obtain

$$\phi = \phi_{eo}\left[\exp\left(-1.225\frac{x}{L_D}\right)\right] \tag{6.19}$$

The equation (6.19) gives the potential profile of a planar surface silicon nitride gate pH ISFET.

Effective Potential

It has been found that the effective electrolyte oxide interface potential appearing in equation (6.19) should not be ϕ_{eo}. Rather, it should be an effective potential which has been found as

$$\phi_{eo\_eff}(x) = \phi_{eo} - \phi(x)$$

Therefore, equation (6.19) can be written as

$$\phi_{eo\_eff}(x) = \phi_{eo}\left[1 - \exp\left(-1.225\frac{x}{L_D}\right)\right] \tag{6.20}$$

The mathematically obtained ϕ_{eo_eff} is further compared with the experimentally obtained effective interfacial insulator electrolyte potential which is obtained by precise positioning of reference electrode and the acquired data using a system described in the following section.

6.4 Experimental set up

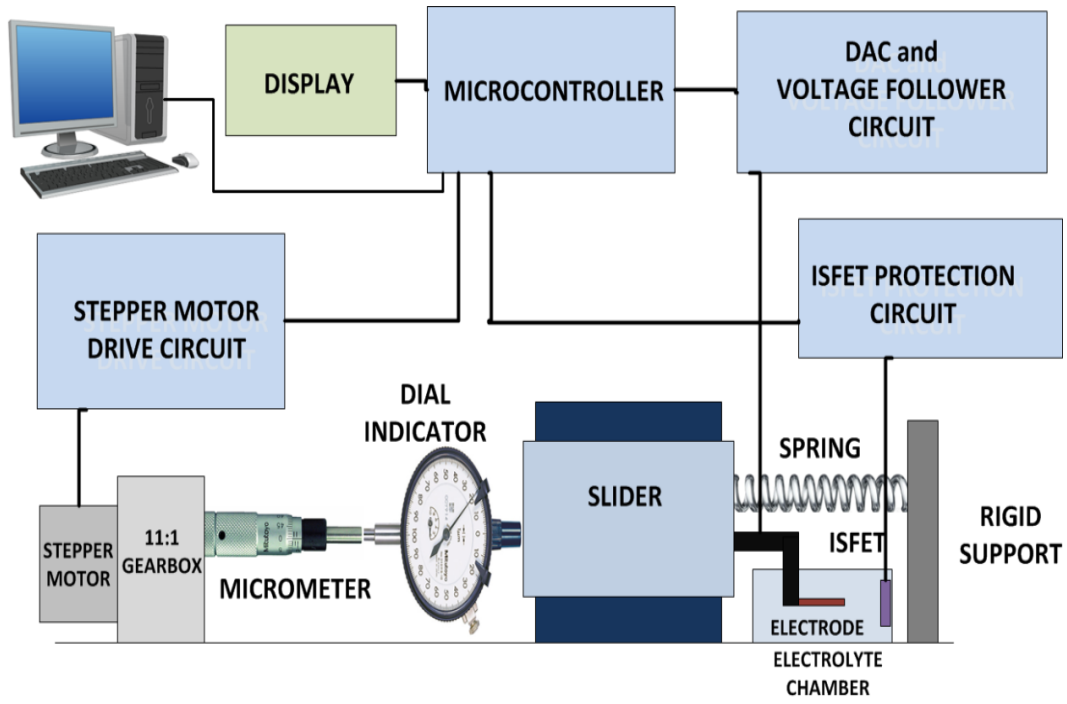

Figure 6.4. Block diagram of the experimental set-up

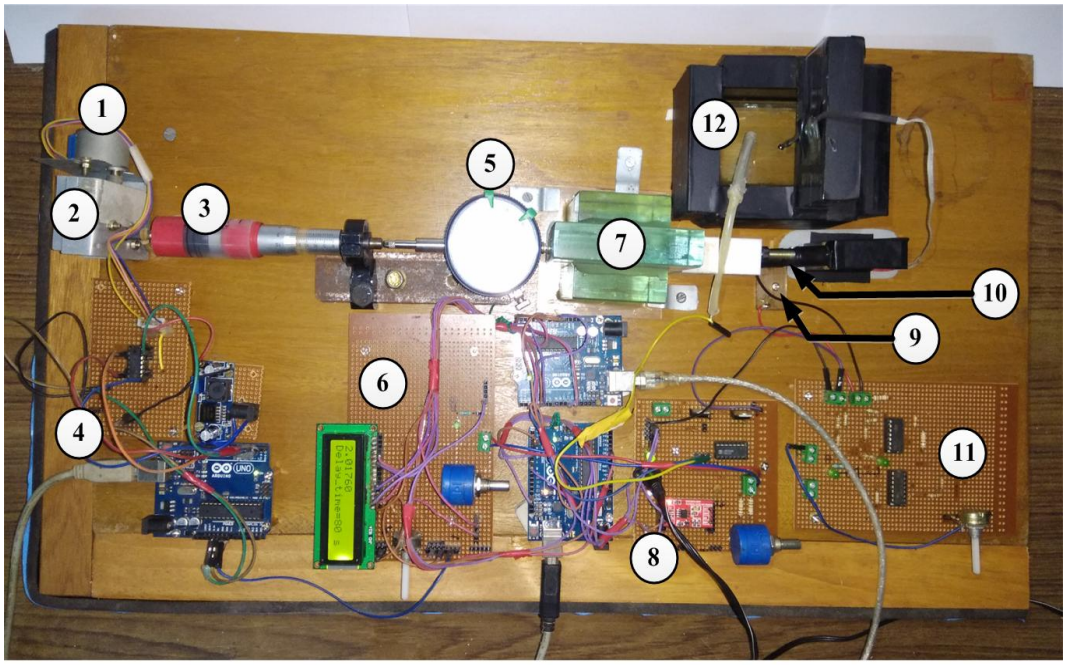

1. Stepper motor
2. Reduction gear box
3. Micrometer
4. Stepper motor driver circuitry
5. Dial indicator
6. LCD along with its circuitry
7. Glass stabilizer
8. Stable voltage generation circuitry
9. Virtual contacts
10. Spring mechanism
11. Protection circuitry
12. Reference electrode along with ISFET immersed in measurand

Figure 6.5. The complete set up with the data acquisition system

The experimental set up has been divided into two major sections, first being the data acquisition system including ISFET biasing circuitry and second is the mechanical system for the precise movement of the reference electrode. Figure 6.4 depicts the block diagram of the set up for the movement of reference electrode along with the necessary data acquisition circuitry. Figure 6.5 illustrates the actual set up along with the data acquisition system. The drain to source voltage to the ISFET was applied using a Keithley Electrometer which is of two electrodes system (figure 6.6).

Figure 6.6. Keithley Electrometer 6517B

A high resolution 10 bit digital to analog converter (DAC) was used to generate a stable voltage at the gate terminal .The DAC was controlled using a microcontroller. The DAC with a resolution of 4.8 mV was used to generate a pulse width modulated (PWM) signal with highly stable amplitude and was later followed by a voltage follower circuit made with an operational amplifier LM324. The presence of the voltage follower circuit avoids any loading effect on the DAC. Part no 8 in figure 6.6 illustrates the stable gate voltage generation circuitry. The voltage stabilized by the voltage follower was then applied to the reference electrode that acts as the gate terminal for the ISFET. Data acquisition was carried out during the ON time of the gate voltage signal and movement of the reference electrode was accomplished during the OFF time as indicated in figure 6.7.

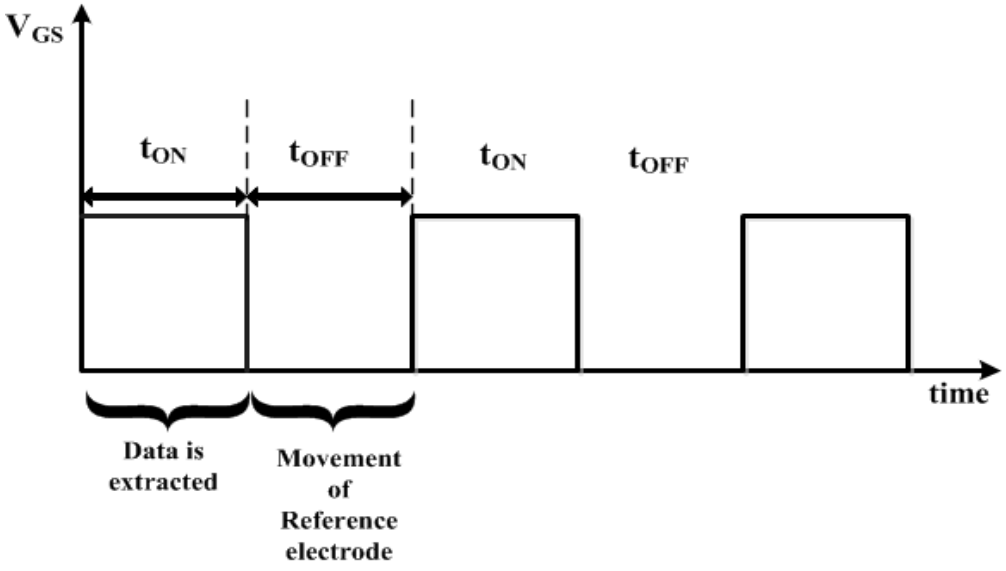

Figure 6.7. The gate voltage signal generated by the DAC

The movement of the reference electrode is required to be completed during the off time of the gate voltage signal for a stable data acquisition process. The discharging time of the gate capacitance varies for different pH and hence the gate signal was programmed to have a variable duty cycle and frequency. The duty cycle of the gate signal was programmed to be varied in real time using a reference voltage provided by a stable 10 kΩ multi turn wire wound potentiometer. During the off period the output of the DAC i.e. the gate voltage was maintained at zero volts and hence a zero drain current was observed. For the convenience, a 16×2 LCD was programmed to display the real time gate voltage generated by the DAC along with the off time of the PWM in seconds(part no 6 in figure 6.6).

The reference electrode was needed to be moved to the desired position while the gate voltage is zero. To accomplish this, the mechanical system was used in synchronization with the data acquisition system. The Debye length varies from 300 to 3000 micrometers for pH 12 to 14. Henceforth the reference electrode must be accurately positioned at various distances from the sensing layer. A micrometer with a least count of 0.2 mm was used for the movement of the reference electrode. With one complete turn of the micrometer's thimble, the spindle (of the micrometer) along with the reference electrode moves forward by a distance of 0.5 mm (500 µm). The thimble of the micrometer was turned using a

stepper motor with necessary gear reduction. With a reduction gear box (figure 6.8) between stepper motor and the micrometer, one degree turn of the stepper motor shaft makes the thimble of the micrometer to turn 0.090 degree. Therefore with one degree turn of stepper motor the spindle and reference electrode move forward by 0.126 µm which is illustrated in figure 6.9. The actual picture of the micrometer and the dial indicator is shown in figure 6.10

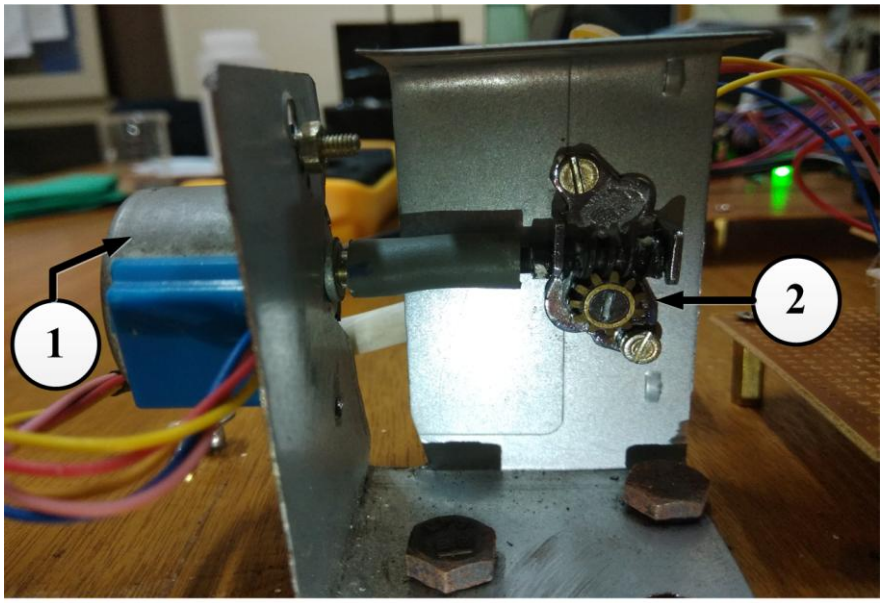

1. Stepper motor
2. Worm gear with 1:11 reduction

Figure 6.8. Stepper motor with 1:11 worm gear reduction

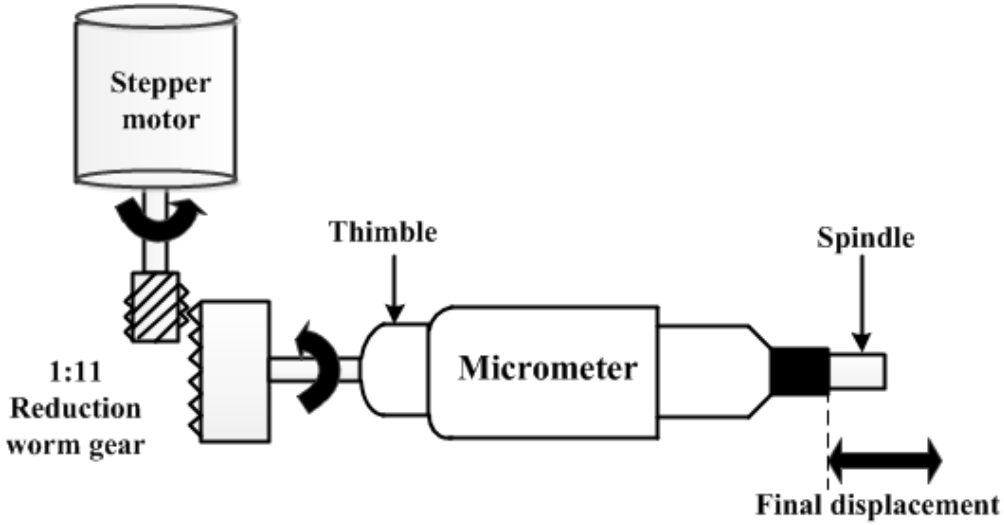

360^0 turn of the thimble = 500 µm final displacement

1^0(movement of thimble of the micrometer) =1.389 µm (final displacement)

1^0 step of stepper motor = 1.389/11 µm displacement of the spindle

= 0.126 µm displacement of the spindle of the micrometer

Figure 6.9. The translation mechanism

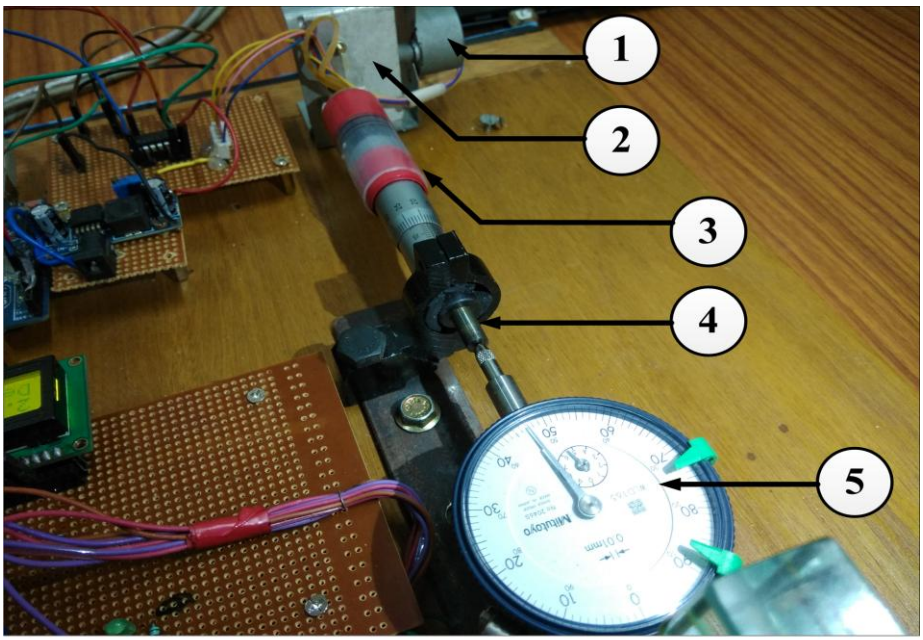

1. Stepper motor **2. Worm gear with 1:11 reduction**
3. Thimble of micrometer **4. Spindle of micrometer**
5. Dial indicator

Figure 6.10. The micrometer and the dial indicator

The precise forward and retrieval movement of the reference electrode was accomplished using a stepper motor (controlled by microcontroller), driven using an H-Bridge IC (L293D). Proper coordination between the two microcontrollers used for the data acquisition and movement of reference electrode was maintained. The ISFET along with the reference electrode was kept immersed in an electrolyte placed in a glass chamber as indicated in figure 6.11.

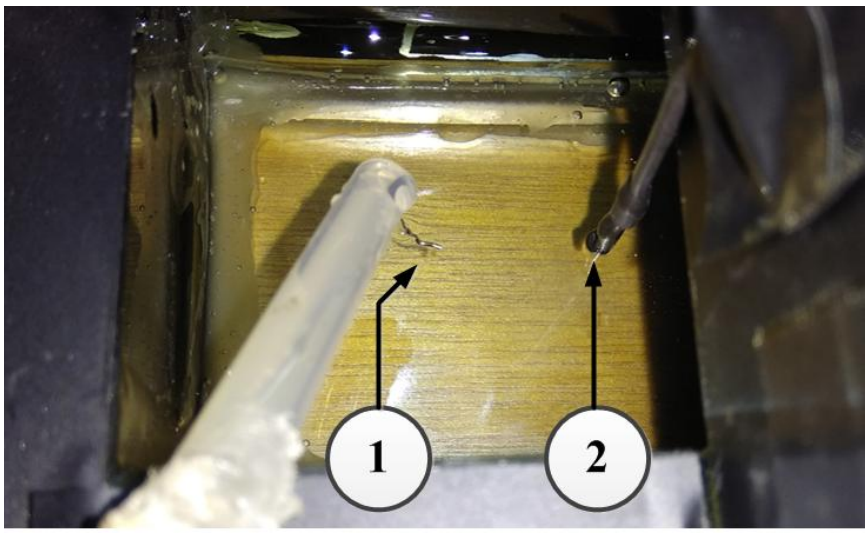

1. Insulated platinum reference electrode with exposed tip
2. Sensing layer of Si_3N_4 ISFET immersed in measurand

Figure 6.11. Reference electrode and the ISFET immersed in measurand

Initially the reference electrode was positioned close to the Silicon Nitrite sensing layer of the ISFET (WINSENSE S01010) and then the reference electrode was moved away using the stepper motor and micrometer assembly discussed above. The reference electrode, if touches the sensing layer of the ISFET can cause permanent damage to the later. To counter this concern, an additional safety measure was employed using mechanical contacts that move in a parallel plane along with the reference electrode. For the lateral stability of the reference electrode a sliding mechanism using glass was designed to ensure the reference electrode movement confined in one dimension (part no 7 in figure 6.5). A dial indicator (Mitutoyo 2046S) was placed between the micrometer spindle and the slider (part no 5 in figure 6.5). The micrometer's spindle pushes the sensor button of the dial indicator and the dial indicator's spindle extended to the diagonally opposite side pushes the slider along with the reference electrode.

In order to prevent any backlash and undesired vibrations in the system a spring (part no 10 in figure 6.5) was compressed during the forward movement of the slider which later helps in the smooth retrieval of the slider along with the reference electrode. Therefore, the complete setup for the movement of reference electrode and data acquisition system is divided into various sub-sections as discussed below. The first and very important component of the setup is the circuitry for the generation of an accurate gate voltage which is applied to the reference electrode. The next section is the circuit for displaying gate voltage using LCD. The next important section illustrates the circuit for the protection of sensing layer, as any impact by the reference electrode on the sensing layer may cause permanent damage to the latter. This is followed by the circuit for driving the stepper motor and its synchronization with the data acquisition system. Finally, the mechanical setup for the precise movement of the reference electrode has been discussed.

6.4.1 Generation of gate voltage

As already indicated earlier, part no 8 of figure 6.5 illustrates the set up for the generation of gate voltage which is applied to the reference electrode. The block diagram and the circuit diagram are illustrated in figure 6.12a and 6.12b respectively.

A 10 bit serial DAC module TLC5615 with a resolution of 4.8 mV was controlled using a microcontroller (Arduino UNO R3) to generate a PWM signal with stable amplitude. The generated voltage from DAC was applied to the voltage follower using an operational amplifier IC LM324 with an input bias current of 20nA. The PWM signal with variable duty cycle was required, as the time required for the discharging of built gate charges may differ for different pH values. The movement of the reference electrode is required to be carried out only during the off time of the PWM as already stated. The off time of the PWM can be varied using a reference voltage from a potentiometer. A LED was used as a visual indicator that provides the information regarding the state of the gate voltage if it was low or high. In addition to this, a 16×2 LCD was used to display the gate voltage along with the time for which it is zero.

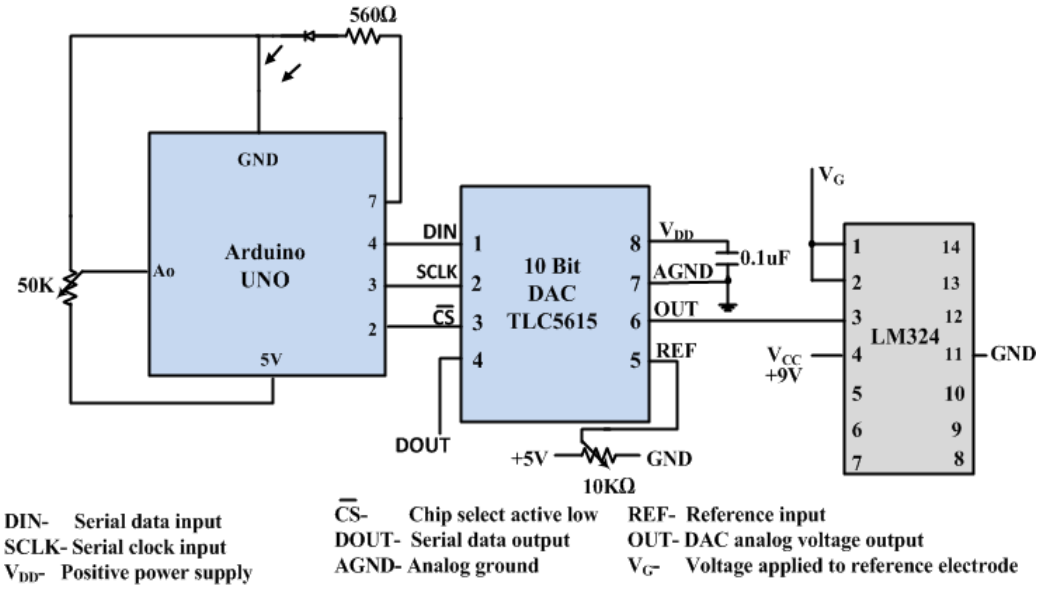

Figure 6.12a. The block diagram for the generation of gate voltage

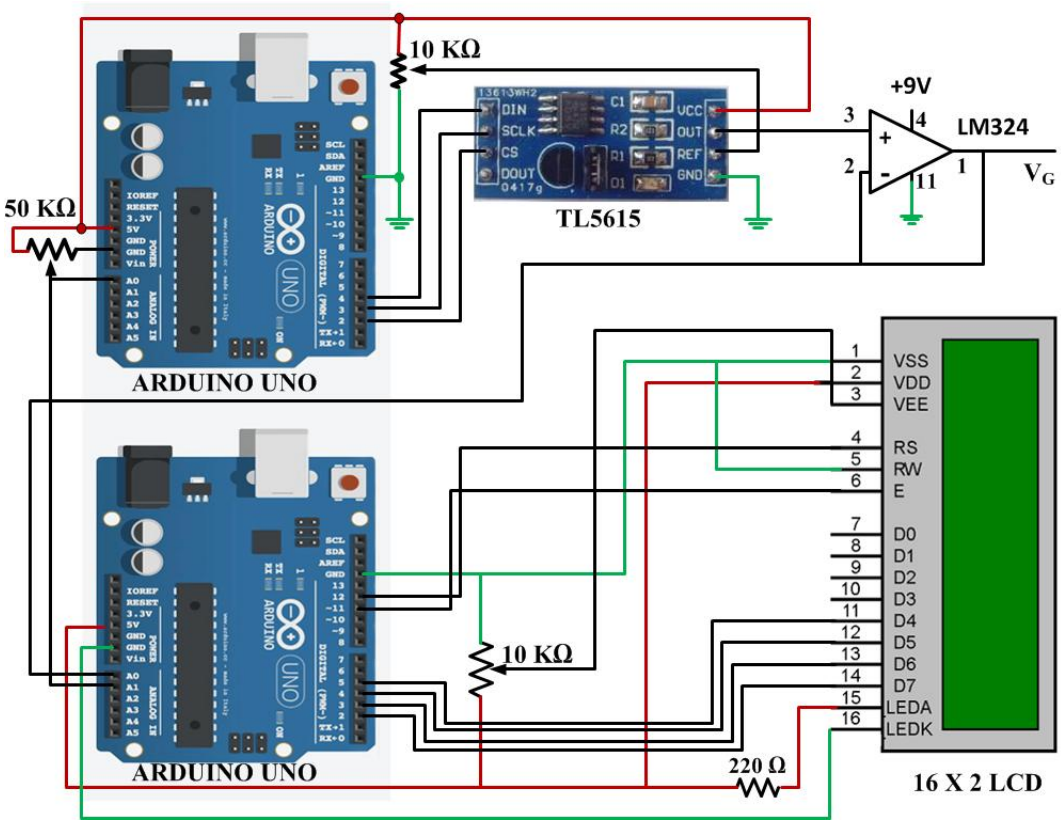

Figure 6.12b Circuit diagram for the generation of the gate voltage and its display in

16×2 LCD

Reference electrode when moved towards the sensing layer, the sensing layer was subjected to a harsh impact that could result in permanent damage of the sensing layer of the ISFET. Henceforth to avoid such a condition a protection system was designed that could avoid any situation that can lead to damage of sensing layer as depicted in figure 6.13 a. As the reference electrode was placed inside the electrolyte hence the microscopic separation between the sensing layer and reference electrode was inconvenient to be inspected. To counter this, separate contact was made to move in parallel with the reference electrode in the same plane. The two contacts acted as the virtual reference electrode (point A, moving along the reference electrode) and sensing layer (point B, stationary) as indicated in figure 6.13 b. Any connection between these external contacts indicated the contact between the actual reference electrode and sensing layer. The distance between the two virtual contacts can be as low as in micrometers hence a higher potential difference between the contacts can lead to high electric field between them and cause dielectric breakdown of the air and can lead to false indication. To avoid this, the potential difference between the two contacts was maintained at 5mV and later amplified to 5V using an op-amp with a gain of 1000. The 5V output was used as the signal to control the movement of stepper motor. Any contact between the virtual reference electrode and sensing layer disabled the motor driver IC (L293D) and aborted any further movement of the reference electrode towards the sensing layer (Figure 6.13 a).

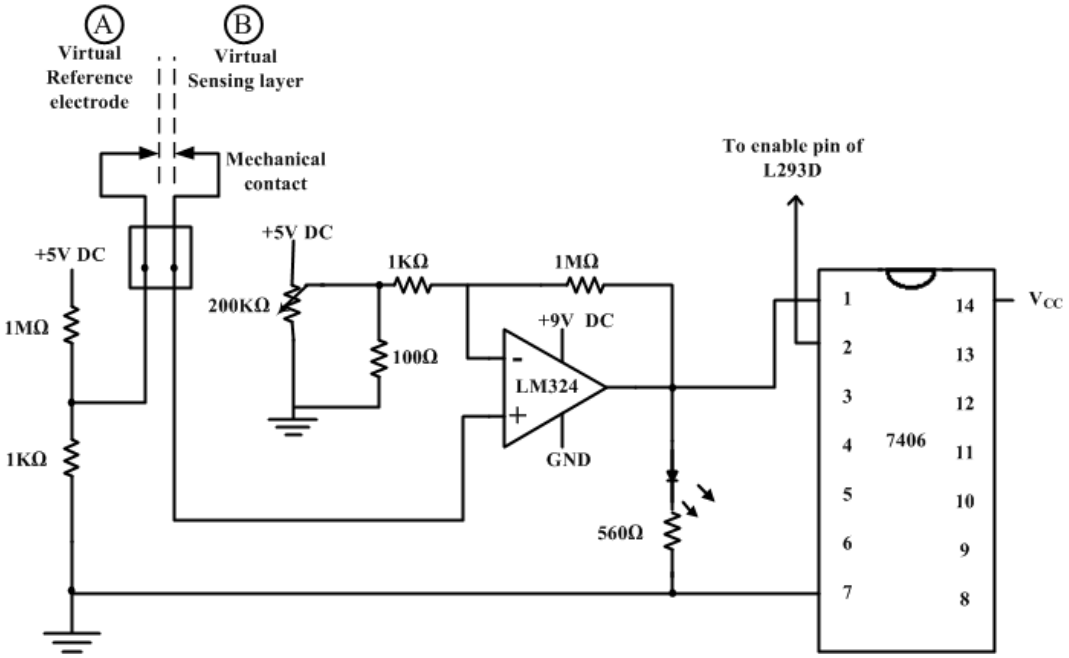

Figure 6.13 a. Protection circuit

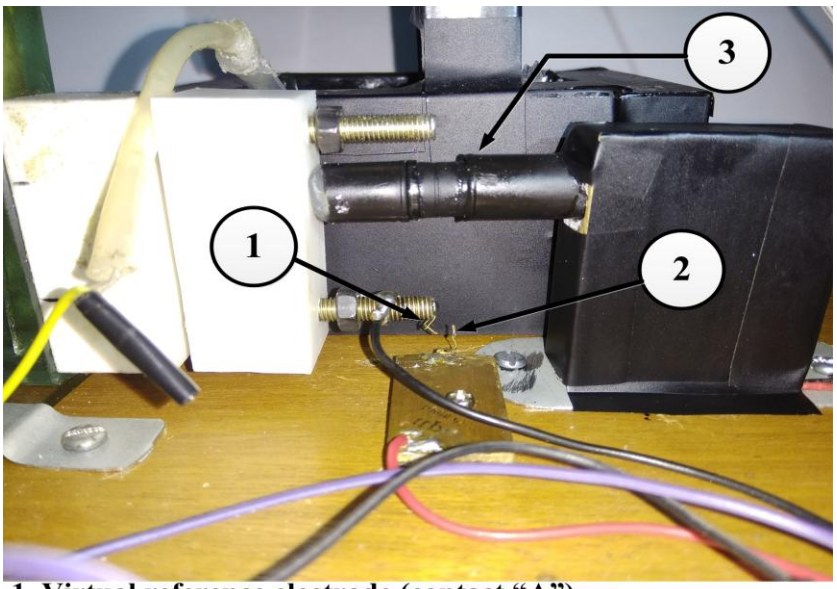

1. Virtual reference electrode (contact "A")
2. Virtual sensing layer (contact "B")
3. Spring mechanism

Figure 6.13 b. Virtual contact points acting as reference electrode and sensing layer along with the spring mechanism

6.5 Results and Discussion

The Debye length along with the pH values for a silicon nitride sensing surface is tabulated in the table 6.1.

Table 6.1. Table for Debye length values for corresponding pH of the measurand for a Si_3N_4 surface

pH value of the measurand	Debye length (in m)
1	9.6484×10^{-10}
2	3.0511×10^{-9}
3	9.6484×10^{-9}
4	3.0511×10^{-8}
5	9.6484×10^{-8}
6	3.0511×10^{-7}
7	9.6484×10^{-7}
8	3.0511×10^{-6}
9	9.6484×10^{-6}
10	3.0511×10^{-5}
11	9.6484×10^{-5}
12	3.0511×10^{-4}
13	9.6484×10^{-4}
14	3.0511×10^{-3}

Further, when the reference electrode is placed in close proximity to the OHP, it has been observed that the potential possesses a higher value. As the electrode is moved far from the OHP into the bulk of the solution, this potential drops gradually. As the pH value increases the charge density attains a negative value which results into negative potential in the vicinity of the sensing layer. It has been observed that the potential has a higher value in the acidic range and it decreases with increase in pH value. This can be explained well by the following plots in figures 6.14 a, b and c. Figure 6.14a is for pH 4, here the charge density is positive. Further, for pH 7, the charge density is negative (figure 6.14b). So is the case for pH 10, where the potential is more negative than in pH 7 as depicted in figure 6.14c. The parameters for the simulation are considered as close as the actual device parameters. The simulation parameters are W=1400 µm, L= 3550 µm and the V_{th} values for pH 12, 13 and 14 are 1.56V, 1.61V and 1.66V respectively, $\varepsilon_0 = 8.854\times10^{-12}$ F/m. For the experimentation, the initial ionic concentration of the pH solution was adjusted to be 0.1 M using a digital pH meter for pH 14. Further, for the consecutive pH solution the initial solution was diluted using Milli Q water.

The system which is developed here has its limitations and can validate the theoretical model only for higher pH values. This limitation of the translational mechanism along with the calculations involved is already indicated in figure 6.9. The effective insulator interfacial potential versus position (in µm) of the reference electrode with respect to the sensing layer for pH 14 is illustrated in figure 6.15 a. In the experiment, a complex mechanical set up was used to position the reference electrode at various distances from the sensing layer. For all pH values the measurements of drain current was carried out with a constant gate voltage of 2V and a constant drain to source voltage of 0.27 V.

Here the plot associated with pH values of 14, 13 and 12 are discussed. The setup is capable of a minimum movement of the reference electrode by 0.126 µm. This limitation as already stated, makes it difficult to carry out this experiment for values below pH 12, as the Debye length of pH values below 12 is beyond the operating range of the design. Three times of Debye length is 9mm for pH 14, henceforth for measurements 90 equidistant points with spacing of 100µm

from the sensing layer were selected as illustrated in figure 6.15b. Initially the reference electrode was positioned in contact with the sensing layer of the ISFET ensuring no damage was done to the latter. The reference electrode was then retrieved back into the bulk of the electrolyte away from the sensing layer. After the steady positioning of the reference electrode the drain current was measured at any desired point by applying gate voltage which was kept at zero when the reference electrode is in motion. ϕ_{eo_eff} can be conveniently derived for all value of the drain current using the threshold voltage equation and the equation defining the drain current for an ISFET device [2, 3]. Thus, ϕ_{eo_eff} was experimentally obtained for each position of the reference electrode. Further it was observed that the theoretically and experimentally obtained values of ϕ_{eo_eff} almost resemble each other. Using the previous equations for pH 14, for pH 13 and 12 the theoretical values is plotted alongside the experimentally obtained value of ϕ_{eo_eff}, for different distances from sensing layer as illustrated in figures 6.16a and 6.16b respectively. It is evident from the figures that the practically acquired value of ϕ_{eo_eff} at any points follows a resembling trend as that of the theoretically derived value of ϕ_{eo_eff} for that point.

It can be observed from figure 6.15a that as the reference electrode touches the sensing surface i.e. x is zero the effective interfacial insulator electrolyte potential becomes zero. The effective potential decreases exponentially when the reference electrode is retraced back from the sensing surface. For pH=14 the ϕ_{eo} is negative (as pH_{PZC}=5.8 [13]). ϕ_{eo_eff} further decreases exponentially with the increase in distance and attains a stable value of -0.567V at three times of the Debye length i.e. 9mm for pH 14. From figure 6.15a it can be observed that at a distance of approximately 9mm from the sensing layer both the experimental and the theoretical plots are in close agreement with each other and attain a stable value, thus clearly indicating that it is redundant to place the reference electrode beyond this distance. Plots associated with pH values 13 and 12 also suggest the same as can be witnessed in figure 6.16a and 6.16b respectively.

Ambiguity in measurement can be the consequence of positioning of the reference electrode within three times the Debye length which can be clearly

observed in figure 6.17. Here in this figure the reference electrode is considered to be positioned at 100µm from the sensing layer and the variation of electrolyte insulator interface potential with pH has been discussed.

For pH =11, the three times of Debye length is 2.88 µm and hence lies well within 100µm whereas for pH values above 11 this 100µm separation is not sufficient to get the complete potential profile for the particular pH value. From the figure 6.17 it is evident that the theoretical curve becomes nonlinear beyond pH 11 and deviates from the ideal case. Also it can be noticed that one value of ϕ_{eo_eff} corresponds to two different values of pH for the curves beyond pH 11, thus leading to ambiguity in measurement. For example ϕ_{eo_eff} = -0.0812V corresponds to pH 7.9 and pH 12.8 of the theoretical curve. Therefore, it can be clearly stated that for accuracy in measurement the position of the reference electrode should be at or beyond the three times of Debye length of each pH values of the measurand.

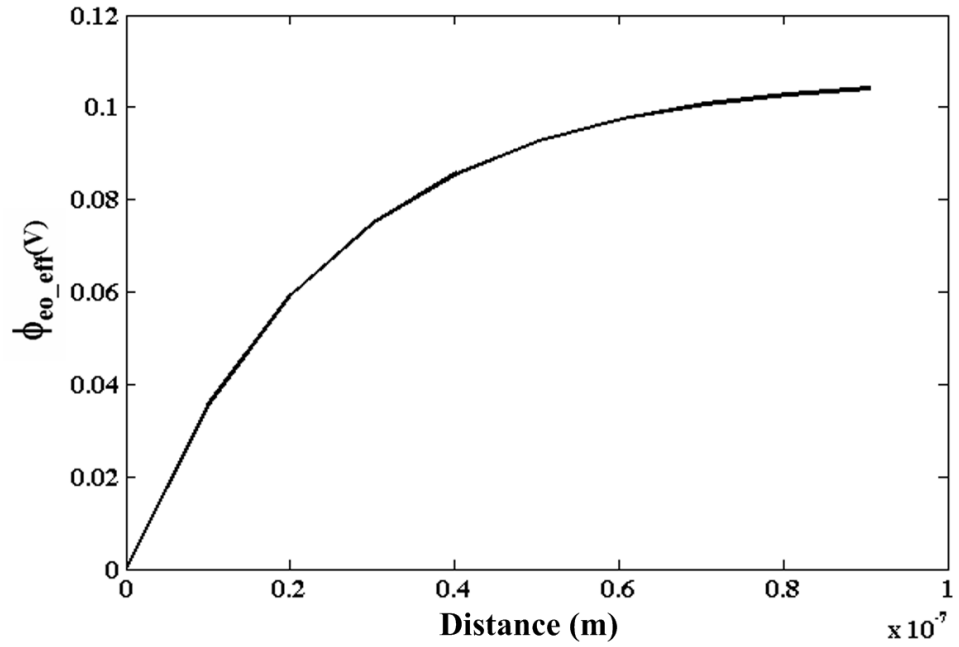

Figure 6.14a. Variation of interfacial effective electrolyte insulator potential with respect to distance for pH 4

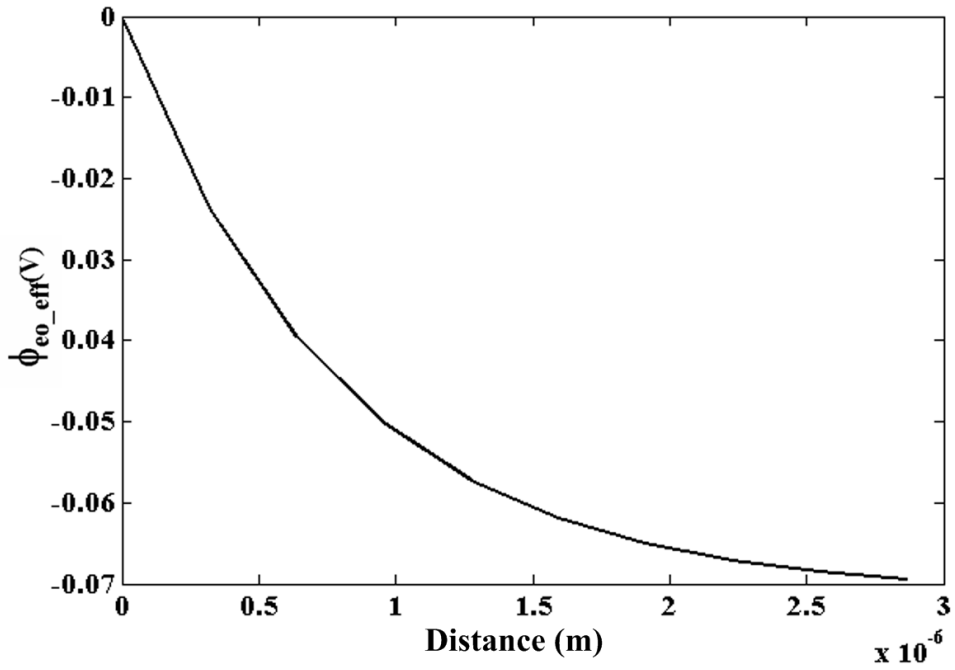

Figure 6.14b. Variation of interfacial effective electrolyte insulator potential with respect to distance for pH 7

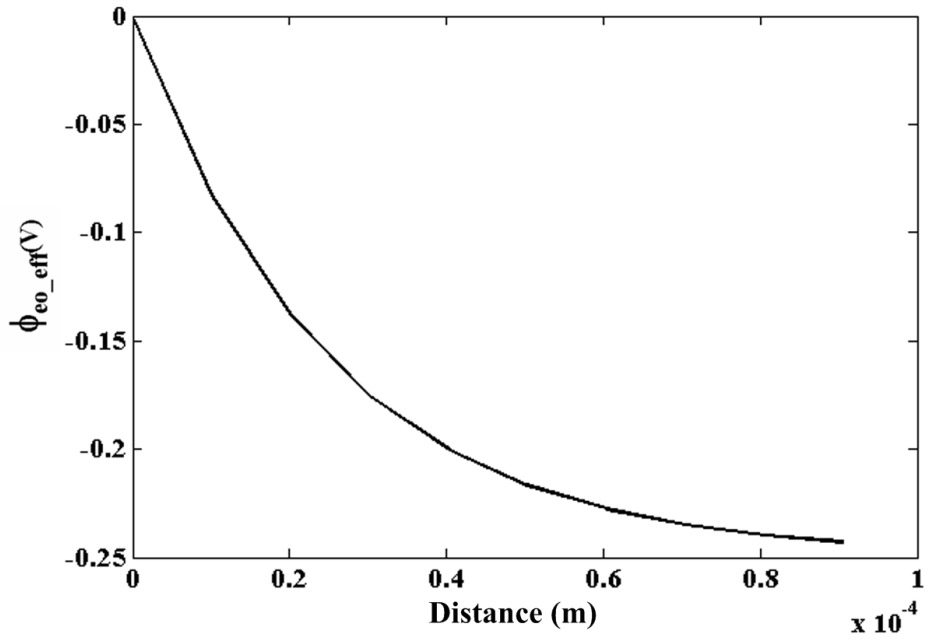

Figure 6.14c. Variation of interfacial effective electrolyte insulator potential with respect to distance for pH 10

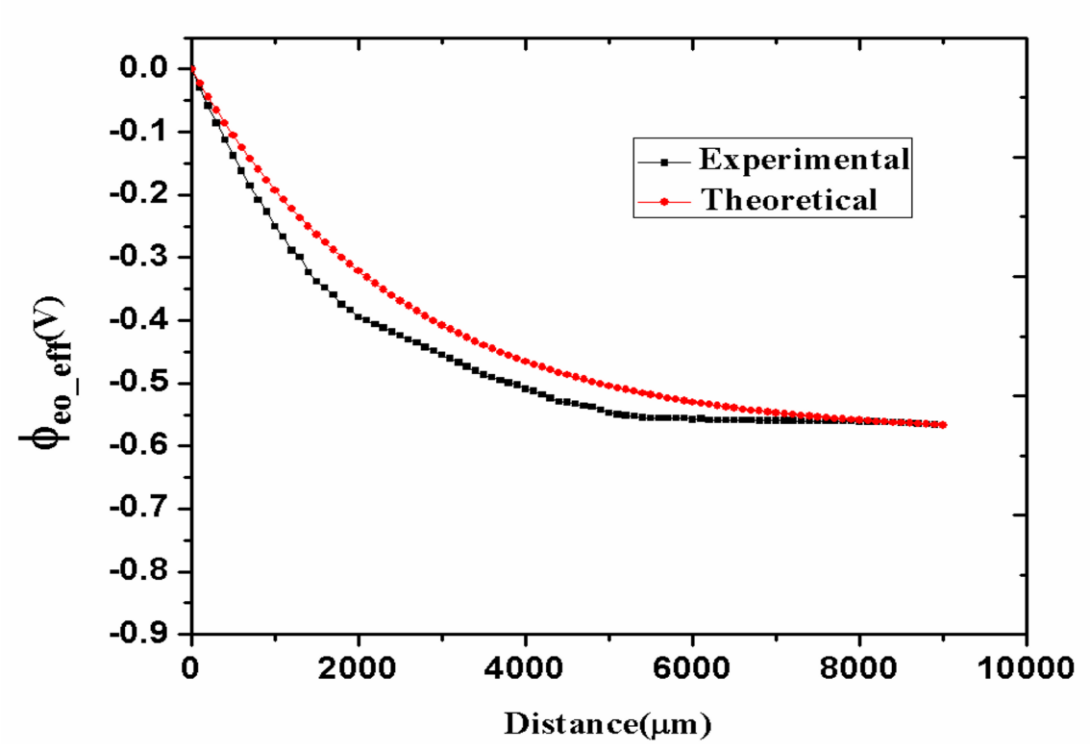

Figure 6.15a.Variation of effective insulator/electrolyte interface potential with increase in distance of the reference electrode from sensing layer ranging from 0 mm (i.e. the sensing layer) to 9 mm (i.e. three times of Debye length for pH 14).

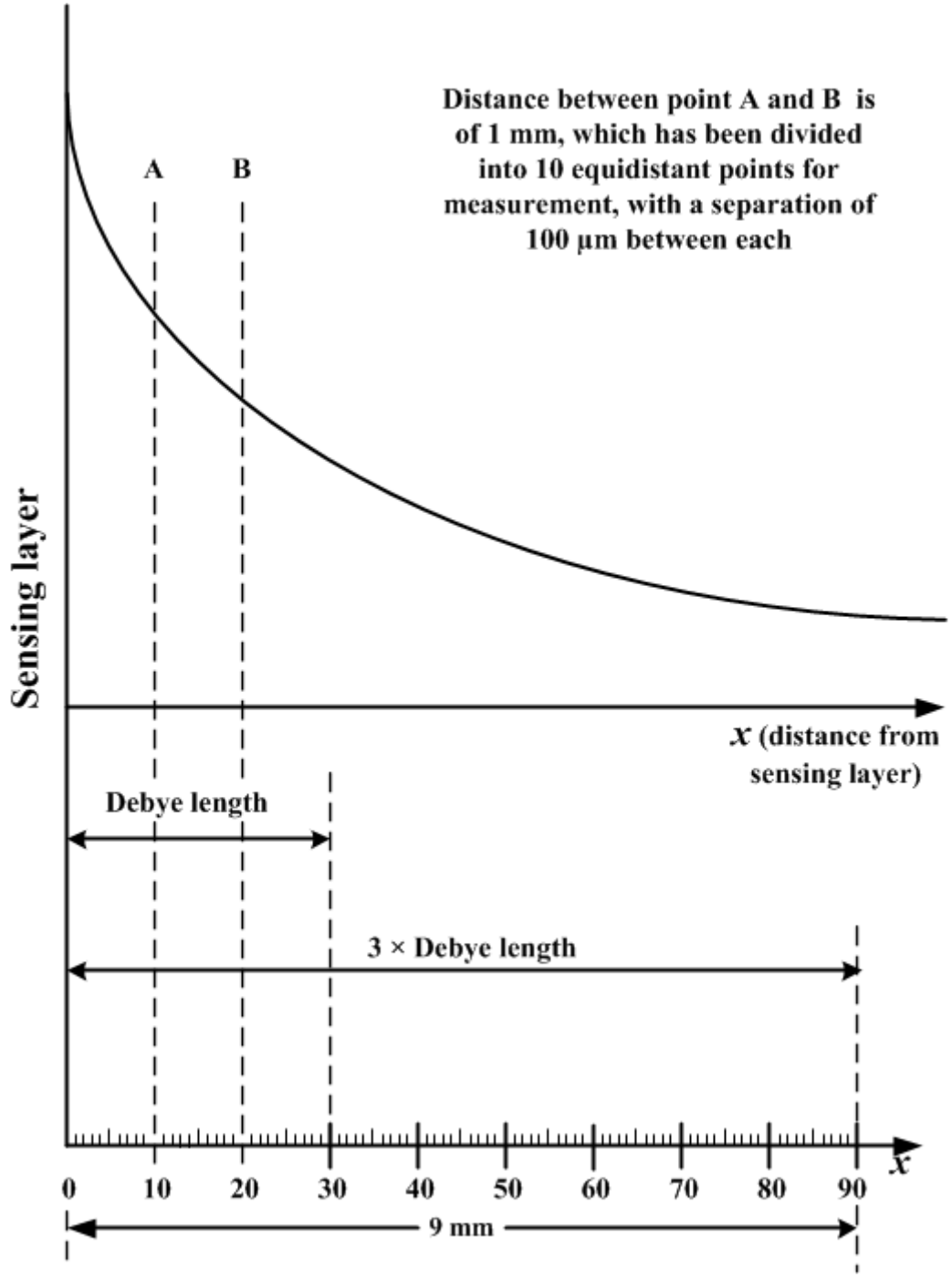

Figure 6.15 b. figure showing 90 different equidistant points between the sensing layer and 3 times of Debye length, chosen for the data extraction for pH 14

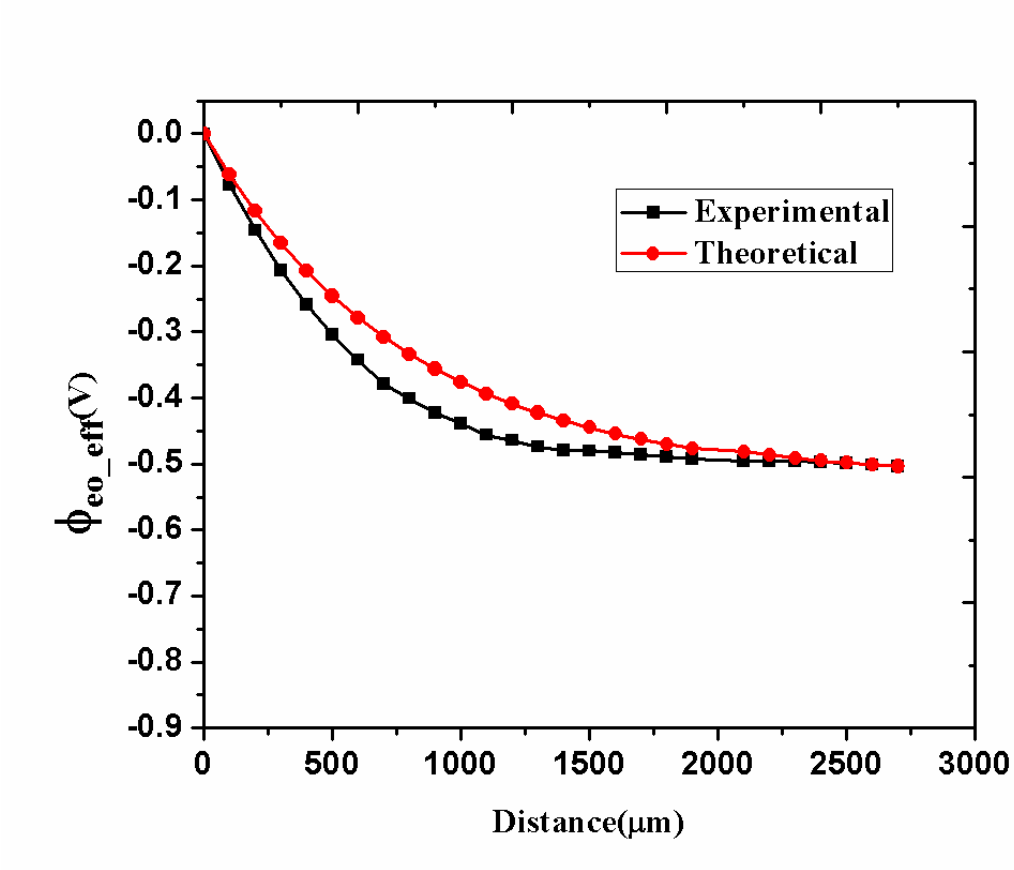

Figure 6.16a.Variation of effective insulator/electrolyte interface potential with increase in distance of the reference electrode from sensing layer ranging from 0 mm (i.e. the sensing layer) to 2.7 mm (i.e. three times of Debye length for pH 13).

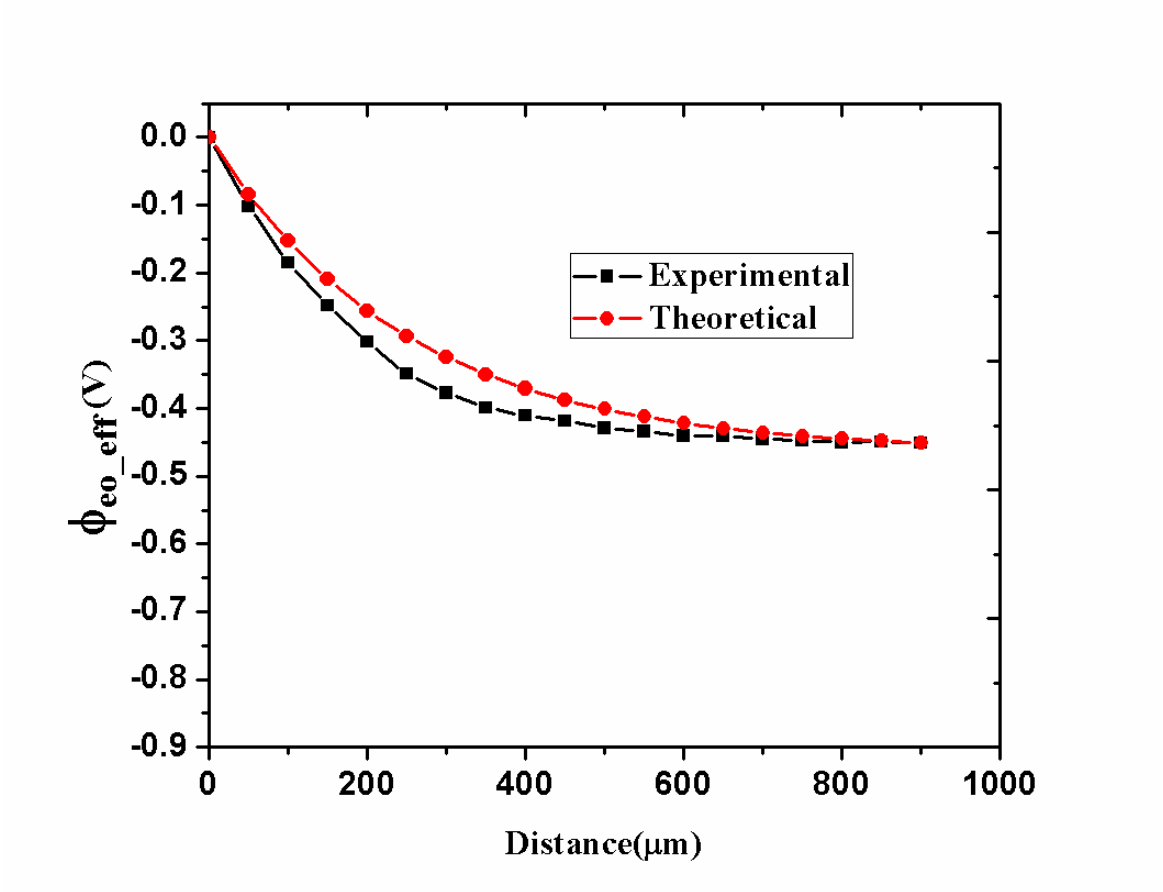

Figure 6.16b.Variation of effective insulator/electrolyte interface potential with increase in distance of the reference electrode from sensing layer ranging from 0 mm (i.e. the sensing layer) to 0.9 mm (i.e. three times of Debye length for pH 12).

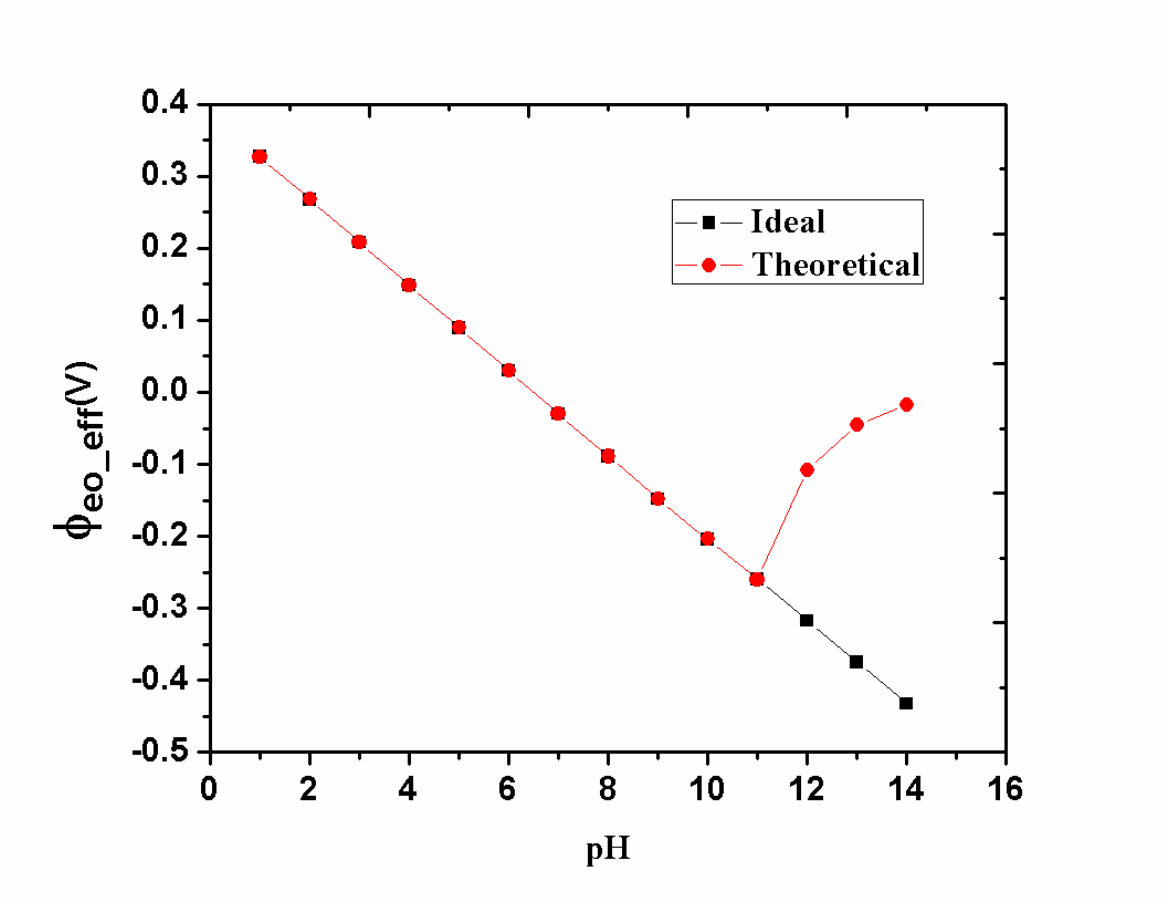

Figure 6.17. Effective insulator electrolyte interface potential (ϕ_{eo_eff}) vs. pH with the reference electrode positioned at 100µm from the OHP.

Bibliography

[1] Sharma, S. *Modeling and Simulation of nanobioelectronic device the cylindrical ion sensitive field effect transistor*, PhD Thesis, Department of Electronics and Communication Engineering, Tezpur University, Tezpur, India, 2009.

[2] Bergveld, P. Thirty years of ISFETOLOGY: What happened in the past 30 years and what may happen in the next 30 years. *Sensors and Actuators B: Chemical*, 88(1):1-20, 2003.

[3] Grattarola, M. and Massobrio, G. *Bioelectronics handbook*, McGraw-Hill, 1998.

[4] Bergström, L. and Pugh, R.J. Interfacial characterization of silicon nitride powders. *Journal of the American Ceramic Society*, 72(1):103-109, 1989.

[5] Harame, D. L., *Integrated circuit chemical sensors*, Ph.D. thesis, Stanford University, Standford, U.S., 1984.

[6] Grattarola, M., Massobrio, G., and Martinoia, S. Modeling H^+-sensitive FETs with SPICE. *IEEE Transactions on Electron Devices*, 39(4):813-819, 1992.

[7] Beruto, D., Mezzasalma, S., and Baldovino, D. Theory and experiments for evaluating the number and the dimensions of solid particles dispersed in a liquid medium. Application to the system Si_3N_4/H_2O (I). *Journal of the Chemical Society, Faraday Transactions*, 91(2):323-328, 1995.

[8] Peri, J.B. Infrared study of OH and NH_2 groups on the surface of a dry silica aero gel. *The Journal of Physical Chemistry*, 70(9):2937-2945, 1966.

[9] Armistead, C.G., Tyler, A.J., Hambleton, F.H., Mitchell, S.A., and Hockey, J.A. Surface hydroxylation of silica. *The Journal of Physical Chemistry*, 73(11):3947-3953, 1969.

[10] Laidler, K. J. *Chemical Kinetics*. McGraw–Hill, New York, 1965.

[11] Mezzasalma, S. and Baldovino, D. Characterization of silicon nitride surface in water and acid environment: a general approach to the colloidal suspensions. *Journal of colloid and interface science*, 180(2):413-420, 1996.

[12] Andelman, D. *Introduction to Electronics in Soft and Biological matter*. Retrieved on 18thSeptember 2017 from http://citeseerx.ist.psu.edu/viewdoc/download?doi=10.1.1.575.2401&rep=rep1&type=pdf, 2004.

[13] Niu, M.N., Ding, X.F., and Tong, Q.Y. Effect of two types of surface sites on the characteristics of Si_3N_4-gate pH-ISFETs. *Sensors and Actuators B: Chemical*, 37(1-2):13-17, 1996.